Vortex Ring Formation in the Left Ventricle of the Heart: Analysis by 4D Flow MRI and Lagrangian Coherent Structures.

Töger, Johannes; Kanski, Mikael; Carlsson, Marcus; Kovács, Sándor J; Söderlind, Gustaf; Arheden, Håkan; Heiberg, Einar

Published in:
Annals of Biomedical Engineering

DOI:
10.1007/s10439-012-0615-3

2012

Vortex ring formation in the left ventricle of the heart: Analysis by 4D flow MRI and Lagrangian Coherent Structures

Running title: Vortex ring formation in the left ventricle

Johannes Töger[1,2], Mikael Kanski[1], Marcus Carlsson[1], Sándor J Kovács[3], Gustaf Söderlind[2], Håkan Arheden[1], Einar Heiberg[1]

[1]Department of Clinical Physiology, Lund University, Skåne University Hospital Lund, Sweden

[2]Department of Numerical Analysis, Centre for Mathematical Sciences, Lund University, Sweden

[3]Cardiovascular Biophysics Laboratory, Department of Medicine, Cardiovascular Division, Washington University Medical Center, St. Louis, MO, 63110 USA

Corresponding author:

Einar Heiberg

Department of Clinical Physiology, Lund University, Skåne University Hospital Lund

221 85 Lund, Sweden

E-mail: einar.heiberg@med.lu.se

Fax: +46-46-151769 Telephone: +46-46-171605

Abstract

Recent studies suggest that vortex ring formation during left ventricular (LV) rapid filling is an optimized mechanism for blood transport, and that the volume of the vortex ring is an important measure. However, due to lack of quantitative methods, the volume of the vortex ring has not previously been studied. Lagrangian Coherent Structures (LCS) is a new flow analysis method, which enables in vivo quantification of vortex ring volume. Therefore, we aimed to investigate if vortex ring volume in the human LV can be reliably quantified using LCS and magnetic resonance velocity mapping (4D PC-MR). Flow velocities were measured using 4D PC-MR in nine healthy volunteers and four patients with dilated ischemic cardiomyopathy. LV LCS were computed from flow velocities and manually delineated in all subjects. Vortex volume in the healthy volunteers was 51 ± 6% of the left ventricular volume, and 21 ± 5% in the patients. Interobserver variability was -1 ± 13% and interstudy variability was -2 ± 12%. Compared to idealized flow experiments, the vortex rings showed additional complexity and asymmetry, related to endocardial trabeculation and papillary muscles. In conclusion, LCS and 4D PC-MR enables measurement of vortex ring volume during rapid filling of the LV.

Key terms: Diastole, diastolic function, 4D flow, LCS, intracardiac, blood flow, magnetic resonance, CMR, hemodynamics

Introduction

During rapid filling (transmitral Doppler E-wave in cardiac ultrasound) of the human left ventricle (LV), a three-dimensional ring-shaped vortex forms downstream from the mitral annulus[7,11,19,28]. Earlier studies suggest that vortex ring formation is connected to diastolic function and overall cardiac health[7,14,26]. Therefore, quantitative measurement of vortex ring attributes may provide additional insight into diastolic function and dysfunction. Earlier studies have described vortex formation in terms of one-directional transmitral flow profiles[7,14] and the movement and rotation of the vortex ring core[13,19]. In a recent review, Dabiri suggested that the volume of the vortex ring is an important property of vortex ring formation, since a large vortex ring can transport a large amount of blood into the LV during diastole efficiently and without forming a turbulent jet[2]. Additionally, the vortex ring may enhance recoil of the atrioventricular plane towards the base of the heart during rapid filling[17]. However, robust methods for defining and measuring the boundaries of the vortex ring in pulsatile flows in vivo have been lacking, and the volume and shape of the vortex ring have not previously been described.

Shadden et al.[30] have suggested that Lagrangian Coherent Structures (LCS), a recently introduced flow analysis method, enable definition of vortex boundaries and therefore measurement of vortex volume. In experiments in water tanks, a distinct LCS pattern can be observed in connection to vortex ring formation (Figure 1)[30,31]. LCS have been shown to agree well with other definitions of vortex ring volume[24,30,31] and have previously been used for cardiovascular applications, both in vivo[21] and in computations[29,32]. However, LCS have never been used to define and measure the volume of the vortex ring in the human LV in vivo.

Therefore, the purpose of this study was to investigate if LCS and 4D PC-MR velocity mapping can be used to describe the vortex ring during early diastolic inflow to the left ventricle (Figure 2). Additionally, we sought to describe the shape of the vortex ring and quantify its size in healthy volunteers and in patients with dilated ischemic cardiomyopathy.

Materials and Methods

Study population and CMR protocol

Nine healthy volunteers and four patients with dilated ischemic cardiomyopathy were included. All healthy volunteers had normal blood pressure, normal ECG and no history of cardiovascular disease. Table 1 shows subject characteristics. The study was approved by the Regional Ethical Review Board in Lund, Sweden. Written informed consent was obtained from all subjects.

All subjects underwent cardiovascular magnetic resonance (CMR) imaging consisting of balanced steady-state free precession (b-SSFP) cine images in 2-chamber, 3-chamber, 4-chamber and short-axis views. Typical parameters: slice thickness 8 mm, in-plane resolution 1.25 x 1.25 mm^2. An experienced observer verified normal anatomy, wall motion and valve function in the healthy volunteers. In the same imaging session, three-dimensional, time-resolved, three-component velocity mapping (4D PC-MR) was performed on all subjects at rest using a three-dimensional Turbo Field Echo (TFE) Phase Contrast sequence[5] on a Philips Achieva 3T CMR scanner. To test interstudy variability, six of the subjects were scanned both on a 3T and a 1.5T Philips Achieva CMR scanner on the same day in random order. The following parameters were used on both scanners: Spatial resolution $3 \times 3 \times 3$ mm^3 (acquired and reconstructed), flip angle 8°, TE 3.7 ms, TR 6.3 ms, velocity encoding

(VENC) 100 cm/s, temporal resolution 50 ms, SENSE = 2 and turbo factor = 2. Respiratory gating and retrospective ECG-triggering was used.

First-order phase background correction and phase unwrapping was performed using a custom plug-in to the software package Segment[12]. Concomitant gradients were compensated by the CMR scanner.

Definition of cardiac cycle events and LV volumes

The definition of cardiac cycle events and the corresponding LV volumes are described in Figure 3. The top panel of Figure 3 illustrates how the volume of the left ventricle (LV) varies over the cardiac cycle, and the associated volume measurements. Ejection fraction (EF) was defined as stroke volume (SV) divided by end-diastolic volume (EDV). The onset of diastole was physiologically defined as the time of smallest blood pool area in a mid-ventricular short-axis image. The bottom panel of Figure 3 illustrates how the timing of the end of rapid filling, diastasis and onset of atrial contraction were determined. Flow through a plane just above the mitral annulus in the left atrium was reconstructed from the 4D PC-MR flow data. The slope between 25% and 75% of maximum flow during rapid filling and atrial contraction was extrapolated to zero to find the end of rapid filling (Dt1, early diastasis) and onset of the atrial contraction (Dt3, late diastasis) respectively. The duration of diastasis was defined as the time between Dt1 and Dt3. Mid-diastasis (Dt2) was defined as the time halfway between Dt1 and Dt3.

Computation of Lagrangian Coherent Structures

To describe the shape of the vortex ring and measure its volume, Lagrangian Coherent Structures (LCS) were computed in each image plane and time phase during diastole as described in previous studies[30,32]:

1) The three-dimensional and time-resolved 4D PC-MR velocity data were interpolated linearly in time and space to produce a continuous velocity field **v**(**x**, *t*), where **x** is the three-dimensional spatial coordinate in the 4D PC-MR field of view, measured in meters and *t* is the time, counted in seconds from the electrocardiogram R-wave.

2) The time-dependent motion of a particle **x**(t) in the flow was assumed to be governed by the differential equation

$$\dot{\mathbf{x}}(t) = \mathbf{v}(\mathbf{x}(t), t)\,. \qquad (1)$$

3) Let $\phi_t^{t_0}(\mathbf{x}) : \mathbf{x}(t) \mapsto \mathbf{x}(t_0)$ denote the flow map, which maps fluid particles from their location at time *t* (Dt1, Dt2 or Dt3) to time t_0 (onset of diastole). A rectangular grid of particles spaced 0.8 mm apart in the plane and 0.8 mm above and below each plane was considered. The flow map was computed for each point in the grid by integrating Eq. (1) with a fourth-order Runge-Kutta method with time step 5 ms, from time *t* backwards in time to t_0. Hence, the computed LCS capture the vortex formation, from onset of diastole until one of the three time phases Dt1 (end of E-wave), Dt2 (mid-diastasis) and Dt3 (end-diastasis, onset of A-wave).

4) The finite-time Lyapunov exponent (FTLE) $\sigma(\mathbf{x}, t, t_0)$ was computed using the formula[30]

$$\sigma(\mathbf{x}, t, t_0) = \frac{1}{|t - t_0|} \ln \left\| \frac{d\phi_t^{t_0}(\mathbf{x})}{d\mathbf{x}} \right\|_2 . \qquad (2)$$

The linearization of the flow map $d\Phi/d\mathbf{x}$ was computed by centered finite differences with neighboring grid points in each direction.

Steps 1-4 were performed in the 2-, 3,- and 4-chamber long-axis views and in short-axis planes spaced 4 mm apart. FTLE values were normalized to the 95th percentile of

FTLE values in the images in each time phase. Lines with FTLE values higher than 50% of this value were considered as LCS.

Manual delineations

LV end-systolic volume (ESV), end-diastolic volume (EDV) (see Figure 3) and diastatic volume (DV, at Dt1, Dt2 and Dt3) were determined by manually drawing contours of the blood volume in short-axis slices covering the LV. The volume for each slice was computed as the area inside the delineation times the distance between slices (8 mm), and the total blood volume was determined as the sum of the volumes in all slices. Stroke Volume (SV) was then computed as the difference between EDV and ESV, and E-wave volume (EWV) as the difference between DV and ESV (see Figure 3).

Vortex volume (VV) was determined as follows. First, LCS indicative of vortex ring formation were delineated in the long-axis views. Since the trailing edge of the vortex ring could not be identified in our data, the leading edge was continued to the atrioventricular plane along the LCS originating from the mitral valve leaflets (Figure 4, panels C and E). Vortex ring volume was then delineated in the computed short-axis slices 4 mm apart, guided by the long-axis delineations. Total vortex volume was computed by summing the volume contribution of each slice as described for ESV, EDV and DV above. Example delineations in one long-axis and one short-axis slice are shown in Figure 4, Panels C and D.

Vortex volume in relation to LV diastatic volume (DV), VV%, was defined as VV divided by DV. For subjects with a diastasis longer than 100 ms, LCS were delineated at the end of rapid filling (Dt1), mid-diastasis (Dt2) and onset of atrial contraction (Dt3). A diastasis shorter than 100 ms was considered too short to reliably perform three separate measurements, and therefore LCS were only delineated at the end of

rapid filling (Dt1) in those subjects. In the six volunteers where measurements at 1.5T were available, vortex ring volume was delineated at Dt1 to test variability between scanners and separate examinations of the same subject.

Two observers delineated vortex ring LCS independently to test if vortex volume (VV) can be objectively determined from the LCS images. Interobserver variability was defined as the difference in vortex volume (VV) between the two observers and was computed at each of the three time phases.

Vortex formation ratio

Vortex formation ratio[8] (VFR), also called stroke ratio (L/D) or vortex formation time (VFT), was computed using the formula[7,14]:

$$\mathrm{VFR} = \frac{4}{\pi} \times \frac{\mathrm{EWV}}{\mathrm{SV}} \times \frac{\mathrm{EDV}}{D^3} \times \mathrm{EF} = \frac{4}{\pi} \times \frac{\mathrm{EWV}}{D^3}.$$

EWV was computed from short-axis manual delineations as described above. The diameter of the mitral valve *D* was computed as the average of the maximal observed distance between the leaflet tips during the rapid filling phase, perpendicular to the flow direction, in the three-chamber view and the distance between the commissures as seen in a short-axis slice through the mitral valve.

Statistical analysis

Bias was computed using Bland-Altman analysis. Differences in VV between observers, studies and time points and DV between time points were tested using the Wilcoxon test. Differences in VV% and VFR between the healthy subjects and patients were tested using the Mann-Whitney U test. P-values <0.05 were considered statistically significant.

Results

Flow measurements using 4D PC-MR were successful in all subjects. Lagrangian Coherent Structures (LCS) indicative of vortex ring formation in the left ventricle

were observed in the 3-chamber view in all 9 healthy volunteers and 4 patients. Vortex ring LCS were also observed in the 2-chamber view in five healthy volunteers (56% of the volunteers), and in the four-chamber view in one healthy volunteer (11% of the volunteers) and one patient (25% of the patients). Figure 4 shows a typical example of LCS observed in the left ventricle of the volunteers after rapid filling (Dt1). The LCS were similar to those reported from experiments in water tanks[30,31], but showed additional complexity and adaptation to papillary muscles and trabeculation (Figure 4 F, asterisks (*)). Figure 5 shows a typical example of LCS in the left ventricle of the patients with dilated ischemic cardiomyopathy, at the end of rapid filling (Dt1). Qualitatively, LCS were similar to those found in healthy volunteers, but the vortex ring occupied a smaller part of the LV. Visually, LCS became more complex at Dt2 and Dt3 compared to Dt1 in all subjects (Figure 6).

Animations of vortex ring LCS formation for all 9 healthy volunteers and 4 patients are available as supplemental files, including timing information. In the healthy volunteers, the LCS field originates from the left atrium and mitral valve in the early stages of rapid filling, and later rolls up into a spiral structure. The LCS patterns expand and remain close to the endocardial surface as blood flows into the LV. During diastasis, the LCS patterns become more complex, losing the clear vortex ring structure. In the patients, vortex ring LCS formation is similar to the healthy volunteers. However, in contrast to the healthy volunteers, vortex ring LCS patterns and the endocardial surface remain separated throughout vortex ring formation. During diastasis, the vortex ring LCS contact the LV lateral wall before losing the vortex ring structure.

In 6 out of 9 healthy volunteers (67%) and in 3 out of 4 patients (75%), the duration of diastasis exceeded 100 ms (Group 1), and LCS delineation and diastatic volume

delineations (DV) were performed at the end of rapid filling (Dt1), at mid-diastasis (Dt2) and before atrial contraction (Dt3). The remaining subjects (3 volunteers, 33%, and 1 patient, 25%) had a diastasis shorter than 100 ms (Group 2), and LCS vortex volumes and LV volumes were delineated only at the end of rapid filling.

LV volumes, ejection fraction (EF) and vortex formation ratio (VFR) are presented in Table 2. There was no statistically significant difference in VFR between healthy volunteers and patients (4.5 ± 1.2 vs. 3.3 ± 1.0, p = 0.11). Compared to Dt1, diastatic volume (DV) in the volunteers was 1 ± 3 ml larger at Dt2 (1 ± 2%, p = 0.69), and 4 ± 3 ml larger at Dt3 (2 ± 1%, p = 0.03) in Group 1. Vortex volume (VV) is presented in milliliters and in relation to LV diastatic volume (VV%) in Table 3. At Dt1, VV was 83 ± 20 ml in the healthy volunteers and 74 ± 18 ml in the patients (p = 0.60), and VV% was 51 ± 6% in the healthy volunteers and 21 ± 5% in the patients (p = 0.0028). Individual data for each subject are available online in the supplemental files.

Interstudy and interobserver variability are presented in Table 4. At Dt1, interobserver variability was -1 ± 13% in the volunteers and -7 ± 11% in the patients. The difference between EWV and VV at Dt1 was 8 ± 16 ml (8 ± 17%, p = 0.3) in the volunteers. Interstudy variability between 1.5T and 3T in the volunteers was -2 ± 12% (n = 6, p = 1).

Discussion

In this study, Lagrangian Coherent Structures (LCS) computed from 4D PC-MR data were used to describe and quantify vortex ring formation during rapid filling of the left ventricle (LV). LCS patterns reflecting vortex ring formation were present in all subjects.

Vortex ring formation

Vortex ring LCS observed in this study showed additional complexity compared to idealized water tank experiments[30,31], including variation between the long-axis views and adaptation to trabeculation and papillary muscles. The variation between the different long-axis views may be a consequence of the asymmetry of flow in the left ventricle, subject to the asymmetry of the heart as a whole[18], e.g. the off-center location of the mitral annulus relative to the long-axis of the LV. The vortex ring originates from the left atrium and the mitral valve leaflets, whose asymmetry is likely a major cause for the asymmetry of the vortex ring, and explains the absence of vortex ring LCS patterns in the four-chamber and two-chamber views in some subjects. Visually, the main difference between LCS flow patterns in healthy volunteers and patients is that while the LCS surface remains close to the endocardium in the healthy subjects, they remain substantially separated in the patients. This suggests that endocardial motion and blood flow are matched in the healthy volunteers, in contrast to the patients with dilated ventricles. The LCS field observed in the LV originates from the left atrium and mitral valve in all subjects, which confirms theory and experimental observations in water tanks where vorticity is generated in the shear layer on the inside of the nozzle generating the vortex ring[4].

The clear vortex ring LCS formed after rapid filling and the more complex LCS in later phases of diastole, shown in Figure 6, reveals that vortex ring formation primarily occurs during rapid filling (Doppler E-wave), and that the less organized residual swirling during diastasis does not add volume to the ventricle nor to the vortex structure. This is in line with an earlier study by Kim et al.[19], where vorticity was predominantly observed during rapid filling. LCS may also be influenced by low velocity-to-noise ratio in late diastole[27].The vortex ring volume accounted for approximately half of the diastatic LV blood volume in healthy volunteers and the

vortex ring LCS remained close to the expanding endocardium. This reveals that a large part of the LV blood volume is involved in vortex formation in the healthy heart. Notably, a smaller part of the LV blood volume was involved in vortex formation in the patients with dilated ischemic cardiomyopathy. The motion of blood in diastolic inflow vortex ring may contribute to reducing the likelihood of thrombus formation within the vortex itself and on neighboring structures. A higher risk of thrombus formation has been observed in patients with dilated ventricles and low EF[33], which may be connected to the flow conditions in the patients, with smaller vortex rings that do not extend to the endocardial surface. This may also be relevant in other situations where vortex formation is modified, such as for implanted mitral valves, or obstructed, such as in left ventricular non-compaction.

The constancy of vortex volume and diastatic volume in the healthy volunteers (Group 1, diastasis > 100 ms) at the end of the E-wave, mid-diastasis and before atrial contraction independently confirms the physiologic role of LV volume at diastasis as the equilibrium volume of the LV[34]. Hence, the present results reinforce the view that vortex formation is causally connected to rapid filling (Doppler E-wave), which is a known consequence of overall diastolic function characterized by load, relaxation and stiffness[20]. Earlier studies have demonstrated the relationship between vortex formation and LV chamber properties[9], suggesting that the inflow vortex ring may provide sensitive and specific measures of diastolic function and dysfunction.

In contrast to earlier studies,[7,14,26] VFR was not significantly lower in the patients compared to healthy subjects. However, these previous included a larger number of subjects.

Methodological considerations

The acceptable interobserver variability at the end of rapid filling and somewhat higher variability in the later phases of diastasis can be explained by the more complex LCS in later phases of diastole. The constant vortex volumes throughout the different time phases suggest that vortex size is best measured at the end of rapid filling, i.e. the onset of diastasis. In the present study, only the volume of the vortex ring as defined by LCS was quantitatively studied. Using the vortex boundary delineation provided by LCS in combination with particle tracing[6], other quantitative measures such as fluid entrainment[24] may be computed. Recent studies have also suggested that vortex formation is linked to the load, stiffness and relaxation of the LV during rapid filling in humans[9], and to LV pressure drop and the movement of the mitral annulus in heart-like phantoms[15,16].

E-wave volume (EWV) and vortex volume (VV) did not differ significantly. However, water tank experiments show that vortex rings consist of the inflowing volume plus a volume of surrounding fluid that is entrained during vortex formation[23]. In the LV inflow setting, this suggests that VV should be significantly larger than EWV, which is not confirmed by the present data. However, VV relies on particle tracing in the 4D PC-MR data for computing LCS. Particle tracing can underestimate flow volumes by 13 ± 11% (computed from values in Eriksson et al.[6]), and therefore no conclusions can be drawn on fluid entrainment using the current method.

The influence of noise and limited spatial and temporal resolution on LCS identification in 4D PC-MR data have not been investigated directly in this study. However, the effects of noise and low resolution have been studied in a computational model by reducing the spatial and temporal resolution in a computer-simulated vortex ring[23]. Lowered temporal and spatial resolution gave an underestimation of vortex volume between 1% and 20%. The same computational study showed that vortex ring

LCS are robust to noise, but large amounts of noise resulted in an underestimation of vortex volume of around 5%[23]. Furthermore, theoretical results suggest that LCS are not sensitive to errors localized in time or space[10]. Computational LCS[23] and our in vivo results are not directly comparable due to differing flow conditions, but an underestimation of vortex volume may be present. The effects of other MR velocity errors such as phase background effects remain to be investigated.

The present analysis uses backward-time LCS, which define the leading edge of the vortex ring. Similarly, forward-time LCS describe the trailing edge of the vortex ring[30,31]. However, the trailing edge could not be observed in this study, which may be related to the low spatial and temporal resolution of current 4D PC-MR sequences.

Compared to previously published ranges of normal EDV, healthy volunteers in this study had larger EDV values. However, normalizing for body surface area (BSA) and considering age and gender of each subject, EDV/BSA in the volunteers was within or slightly above 95% confidence intervals for each age and gender group[1,22].

Physiological significance

The LCS calculations presented in this study confirm and reproduce previously known physiology[25], including:

1) Vortex formation in the left ventricle of the human heart displays additional complexity and asymmetry compared to vortex rings in in-vitro experiments. These differences may be significant when comparing results between idealized flow experiments and in vivo intracardiac blood flow.

2) Active vortex formation ceases at the onset of diastasis[19], confirming that early diastolic vortex formation is a causal consequence of suction initiated rapid filling.

3) Chamber volume during diastasis remains constant in the healthy volunteers, in accordance with the requirement that the volume at diastasis serve as the in-vivo equilibrium volume of the LV[34].

Furthermore, we suggest that large vortex ring size relative to left ventricular size observed in normal subjects and the continued evolution of the vortex ring through diastasis (Figure 6) may minimize stasis and thereby facilitate exchange of blood in the ventricle and near the endocardial wall, preventing thrombus formation. In contrast, the smaller vortex ring size relative to the left ventricle observed in the patients results in a larger volume of static blood, which may increase the risk of thrombus formation.

Limitations

The effect of phase background errors was not investigated. Furthermore, no independent validation of the vortex ring boundary and volume was performed. The authors are aware of three different definitions of vortex ring volume: the streamline method[3], dye injection[24] and LCS[30,31]. All three methods agree in water tank experiments[24,30]. The streamline method is not applicable during the transient formation phase of the vortex ring, which limits its usability in the LV. Dye injection is not feasible for in vivo blood flow in humans. Therefore, LCS was chosen to define the vortex ring boundary and volume in vivo.

Conclusions

This study has shown that Lagrangian Coherent Structures and 4D PC-MR velocity mapping can be used to to delineate the boundary and volume of the vortex ring during rapid filling in the human left ventricle, with fair reproducibility between examinations and fair variability between observers. In healthy volunteers, the vortex ring accounted for 51 ± 6% of diastatic LV volume, but only 21 ± 5% in patients with

dilated ischemic cardiomyopathy. Limitations in imaging such as noise and low resolution may cause an underestimation of vortex volume. Compared to experiments in water tanks, vortex rings observed in the left ventricle (LV) displayed additional complexity and asymmetry, likely due to the proximity of endocardial trabeculation and papillary muscles to the surface to the vortex ring, and asymmetry of the mitral valve and the heart as a whole.

Acknowledgments

Anders Nilsson and Freddy Ståhlberg at the Department of Medical Radiation Physics, Lund University, Lund, Sweden and Karin Markenroth-Bloch, Philips Healthcare, Best, the Netherlands substantially improved the study through many fruitful discussions. Johannes Ulén at the Mathematical Imaging Group, Centre for Mathematical Sciences, Lund University, Lund, Sweden is acknowledged for work on LCS visualizations. Ann-Helen Arvidsson and Christel Carlander at the Department of Clinical Physiology, Skåne University Hospital Lund, Lund, Sweden are gratefully acknowledged for assistance in data collection.

This study was supported by Swedish Research Council grants VR 621-2005-3129, VR 621-2008-2949 and VR K2009-65X-14599-07-3, National Visualization Program and Knowledge Foundation grant 2009-0080, the Medical Faculty at Lund University, Sweden, the Region of Scania, Sweden and the Swedish Heart-Lung Foundation. SJK is supported in part by the Alan A. and Edith L. Wolff Charitable Trust, St. Louis, MO, USA, and the Barnes-Jewish Hospital Foundation, St Louis, MO, USA.

Conflicts of Interest

None.

Abbreviations

LCS	Lagrangian coherent structures

FTLE	Finite-time Lyapunov exponent
EDV	End-diastolic volume (see Figure 3)
ESV	End-systolic volume (see Figure 3)
DV	Diastatic volume (see Figure 3)
SV	Stroke volume (see Figure 3)
EWV	E-wave volume (see Figure 3)
VV	Vortex volume
VV%	Vortex volume relative to LV volume at diastasis (VV/DV)
CMR	Cardiovascular magnetic resonance
4D PC-MR	Four-dimensional (3D + time), three-directional, time-resolved phase contrast magnetic resonance velocity mapping

References

1. Alfakih, K., S. Plein, H. Thiele, T. Jones, J. P. Ridgway, and M. U. Sivananthan. Normal human left and right ventricular dimensions for MRI as assessed by turbo gradient echo and steady-state free precession imaging sequences. *J Magn Reson Imaging* 17:323–329, 2003.
2. Dabiri, J. O. Optimal Vortex Formation as a Unifying Principle in Biological Propulsion. *Annual Review of Fluid Mechanics* 41:17–33, 2009.
3. Dabiri, J. O., and M. Gharib. Fluid entrainment by isolated vortex rings. *Journal of Fluid Mechanics* 511:311–331, 2004.
4. Didden, N. On the formation of vortex rings: Rolling-up and production of circulation. *Zeitschrift für angewandte Mathematik und Physik ZAMP* 30:101–116, 1979.
5. Dyverfeldt, P., J. P. . Kvitting, A. Sigfridsson, J. Engvall, A. F. Bolger, and T. Ebbers. Assessment of fluctuating velocities in disturbed cardiovascular blood

flow: In vivo feasibility of generalized phase-contrast MRI. *Journal of Magnetic Resonance Imaging* 28:655-663, 2008.

6. Eriksson, J., C. J. Carlhäll, P. Dyverfeldt, J. Engvall, A. F. Bolger, and T. Ebbers. Semi-automatic quantification of 4D left ventricular blood flow. *J Cardiovasc Magn Reson* 12:9, 2010.
7. Gharib, M., E. Rambod, A. Kheradvar, D. J. Sahn, and J. O. Dabiri. Optimal vortex formation as an index of cardiac health. *Proc. Natl. Acad. Sci. U.S.A.* 103:6305–6308, 2006.
8. Gharib, M., E. Rambod, and K. Shariff. A universal time scale for vortex ring formation. *Journal of Fluid Mechanics* 360:121–140, 1998.
9. Ghosh, E., L. Shmuylovich, and S. J. Kovács. Vortex formation time-to-left ventricular early rapid filling relation: model-based prediction with echocardiographic validation. *J. Appl. Physiol.* 109:1812–1819, 2010.
10. Haller, G. Lagrangian coherent structures from approximate velocity data. *Physics of Fluids* 14:1851–1861, 2002.
11. Heiberg, E., T. Ebbers, L. Wigström, and M. Karlsson. Three-Dimensional Flow Characterization Using Vector Pattern Matching. *IEEE Transactions on Visualization and Computer Graphics* 9:313–319, 2003.
12. Heiberg, E., J. Sjögren, M. Ugander, M. Carlsson, H. Engblom, and H. Arheden. Design and validation of Segment - freely available software for cardiovascular image analysis. *BMC Medical Imaging* 10:1, 2010.
13. Hong, G. R., G. Pedrizzetti, G. Tonti, P. Li, Z. Wei, J. K. Kim, A. Baweja, S. Liu, N. Chung, H. Houle, and others. Characterization and quantification of vortex flow in the human left ventricle by contrast echocardiography using vector particle image velocimetry. *JACC: Cardiovascular Imaging* 1:705–717, 2008.

14. Kheradvar, A., R. Assadi, A. Falahatpisheh, and P. P. Sengupta. Assessment of transmitral vortex formation in patients with diastolic dysfunction. *J Am Soc Echocardiogr* 25:220–227, 2012.
15. Kheradvar, A., and M. Gharib. Influence of ventricular pressure drop on mitral annulus dynamics through the process of vortex ring formation. *Ann Biomed Eng* 35:2050–2064, 2007.
16. Kheradvar, A., and M. Gharib. On mitral valve dynamics and its connection to early diastolic flow. *Ann Biomed Eng* 37:1–13, 2009.
17. Kheradvar, A., M. Milano, and M. Gharib. Correlation Between Vortex Ring Formation and Mitral Annulus Dynamics During Ventricular Rapid Filling. *ASAIO Journal* 53:8–16, 2007.
18. Kilner, P. J., G. Z. Yang, A. J. Wilkes, R. H. Mohiaddin, D. N. Firmin, and M. H. Yacoub. Asymmetric redirection of flow through the heart. *Nature* 404:759–761, 2000.
19. Kim, W. Y., P. G. Walker, E. M. Pedersen, J. K. Poulsen, S. Oyre, K. Houlind, and A. P. Yoganathan. Left ventricular blood flow patterns in normal subjects: a quantitative analysis by three-dimensional magnetic resonance velocity mapping. *Journal of the American College of Cardiology* 26:224–238, 1995.
20. Kovács, S. J., D. M. Mcqueen, and C. S. Peskin. Modelling Cardiac Fluid Dynamics and Diastolic Function. *Phil. Trans. R. Soc. Lond. A* 359:1299–1314, 2001.
21. Krishnan, H., C. Garth, J. Guhring, M. A. Gulsun, A. Greiser, and K. I. Joy. Analysis of Time-Dependent Flow-Sensitive PC-MRI Data. *IEEE Trans Vis Comput Graph* 18:966-977, 2012.

22. Maceira, A. M., S. K. Prasad, M. Khan, and D. J. Pennell. Normalized left ventricular systolic and diastolic function by steady state free precession cardiovascular magnetic resonance. *J Cardiovasc Magn Reson* 8:417–426, 2006.
23. Olcay, A. B., T. S. Pottebaum, and P. S. Krueger. Sensitivity of Lagrangian coherent structure identification to flow field resolution and random errors. *Chaos* 20:017506, 2010.
24. Olcay, A., and P. Krueger. Measurement of ambient fluid entrainment during laminar vortex ring formation. *Experiments in Fluids* 44:235–247, 2008.
25. Pasipoularides, A. The Heart's Vortex: Intracardiac Blood Flow Phenomena. Shelton: People's Medical Publishing House, 2010, 927 pp.
26. Poh, K. K., L. C. Lee, L. Shen, E. Chong, Y. L. Tan, P. Chai, T. C. Yeo, and M. J. Wood. Left Ventricular Fluid Dynamics in Heart Failure: Echocardiographic Measurement and Utilities of Vortex Formation Time. *Eur Heart J – Cardiovasc Imaging*, 13:385-393, 2012.
27. Ringgaard, S., S. A. Oyre, and E. M. Pedersen. Arterial MR Imaging Phase-Contrast Flow Measurement: Improvements with Varying Velocity Sensitivity During Cardiac Cycle. *Radiology* 232:289–294, 2004.
28. Schenkel, T., M. Malve, M. Reik, M. Markl, B. Jung, and H. Oertel. MRI-based CFD analysis of flow in a human left ventricle: methodology and application to a healthy heart. *Ann Biomed Eng* 37:503–515, 2009.
29. Shadden, S. C., M. Astorino, and J.-F. Gerbeau. Computational analysis of an aortic valve jet with Lagrangian coherent structures. *Chaos* 20:0175120, 2010.
30. Shadden, S. C., J. O. Dabiri, and J. E. Marsden. Lagrangian analysis of fluid transport in empirical vortex ring flows. *Phys. Fluids* 18:047105, 2006.

31. Shadden, S. C., K. Katija, M. Rosenfeld, J. E. Marsden, and J. O. Dabiri. Transport and stirring induced by vortex formation. *Journal of Fluid Mechanics* 593:315-331, 2007.
32. Shadden, S. C., and C. A. Taylor. Characterization of coherent structures in the cardiovascular system. *Ann Biomed Eng* 36:1152–1162, 2008.
33. Sharma, N. D., P. A. McCullough, E. F. Philbin, and W. D. Weaver. Left Ventricular Thrombus and Subsequent Thromboembolism in Patients With Severe Systolic Dysfunction. *Chest* 117:314–320, 2000.
34. Shmuylovich, L., C. S. Chung, and S. J. Kovács. Point: Left Ventricular Volume During Diastasis Is the Physiological in Vivo Equilibrium Volume and Is Related to Diastolic Suction. *J Appl Physiol* 109:606–608, 2010.

Figures

Figure 1 - Lagrangian Coherent Structures in experimental vortex rings

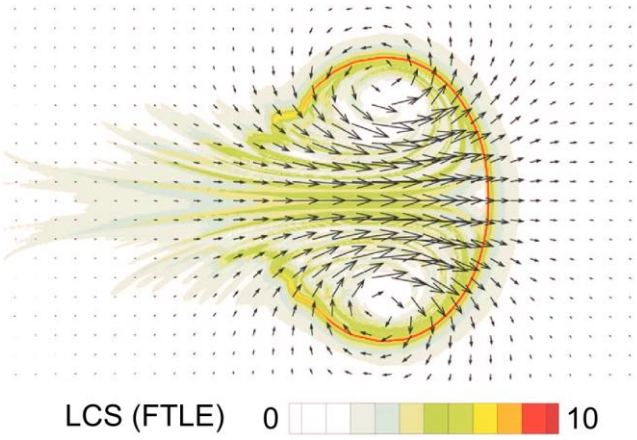

Lagrangian Coherent Structures (LCS) in a vortex ring in water[30]. The vortex ring moves from left to right. Black arrows show flow velocity direction and speed. The red line shows an LCS indicating the leading edge of the vortex. The volume of the vortex ring can be defined as the volume inside the red LCS line. LCS are defined as lines with high values of the Finite-Time Lyapunov Exponent (FTLE), computed from flow data. Adapted with permission from Shadden SC, Dabiri JO, Marsden JE, Phys. Fluids, Vol. 18, 047105, 2006. Copyright 2006, American Institute of Physics.

Figure 2 – Early rapid filling of the left ventricle

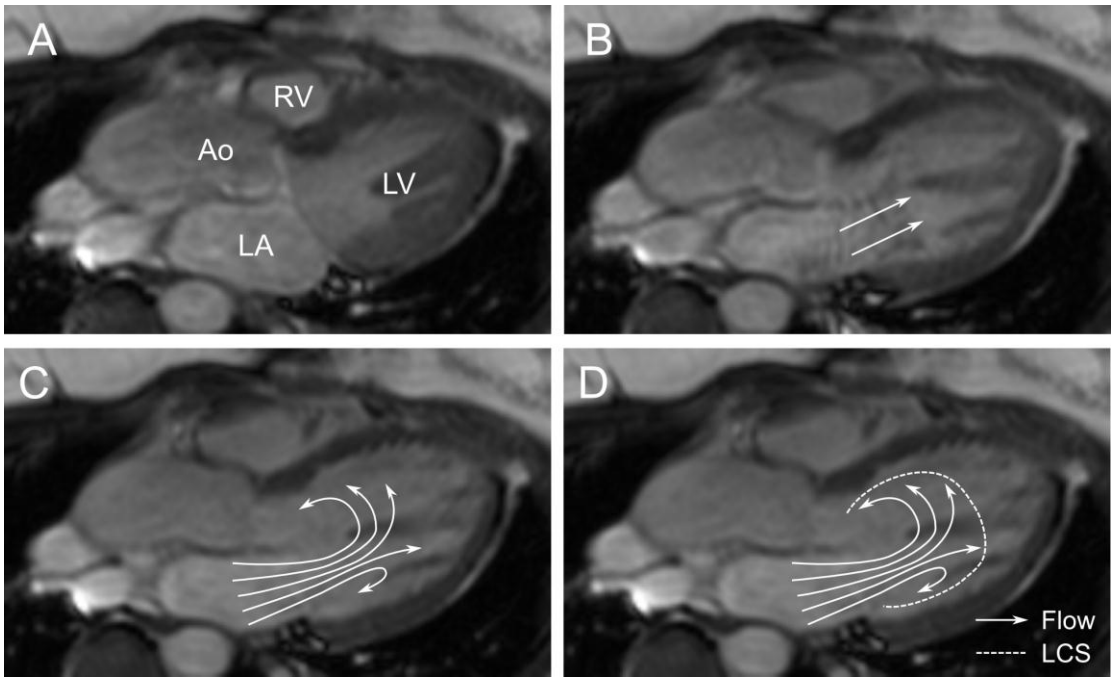

Rapid filling of the left ventricle (LV) of the heart in a three-chamber long-axis view, drawn by hand from particle trace visualizations. In panel A, the LV is at minimum volume, defining the start of diastole, while the mitral valve is still closed. The left atrium (LA), left ventricle (LV), aorta (Ao) and right ventricle (RV) are labeled. Panel B shows the first phase of rapid filling (Doppler E-wave), where blood is aspirated by the LV from the LA. In panel C, rapid filling has progressed, and a three-dimensional, asymmetric, ring-shaped vortex has appeared. The image shows a cross-section of the three-dimensional vortex ring. Panel D shows the hypothesized appearance of Lagrangian Coherent Structures in the LV (LCS, dashed line), delineating the boundary of the vortex ring. See text for details.

White arrows = flow, dashed line = Lagrangian Coherent Structure (LCS).

Figure 3 - Definition of LV volumes and time phases in the cardiac cycle

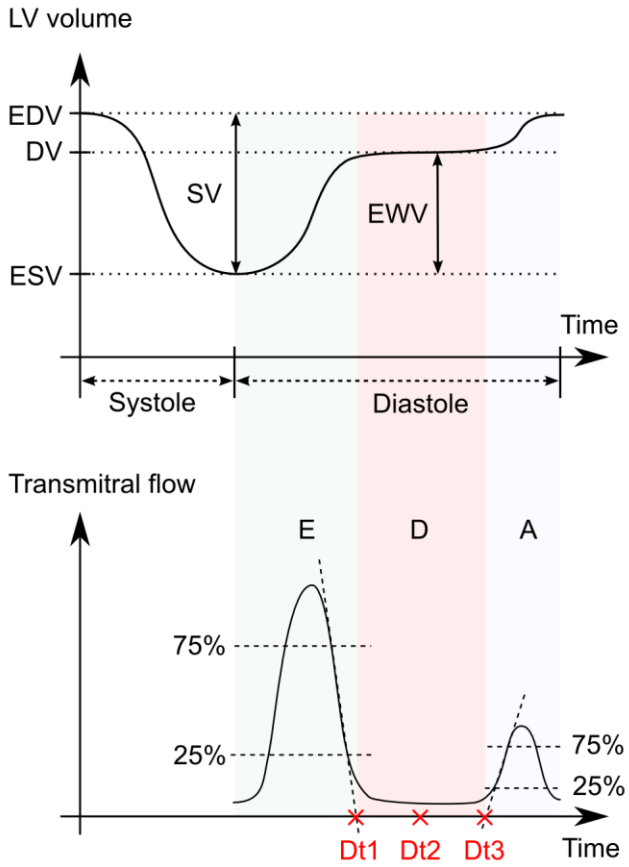

Top: Volume of the left ventricle (LV) during the cardiac cycle. End-diastolic volume (EDV) is defined as the maximum blood volume of the LV, and end-systolic volume (ESV) is the minimum volume of the LV. Diastatic volume (DV) is defined as the volume at diastasis, i.e. after early rapid filling but before atrial contraction. Stroke volume (SV) is defined as the volume ejected from the LV during systole, i.e. the difference between EDV and ESV. The E-wave volume (EWV) is defined as the volume increase of the LV during early rapid filling, i.e. the difference between DV and ESV.

Bottom: The early rapid filling phase (E), diastasis (D) and atrial contraction (A) of the left ventricle were determined by retrospective flow quantification (solid line) in the left atrium in the 4D PC-MR velocity data. The slopes between 25% and 75% of

maximum flow during rapid filling and atrial contraction were extrapolated to zero to define the end of rapid filling and the start of atrial contraction. Red crosses denote the three time points where vortex volume was determined: after rapid filling (Dt1, early diastasis), at mid-diastasis (Dt2) and before atrial contraction (Dt3, late diastasis). Diastasis is defined by the interval between Dt1 and Dt3. See text for details.

Figure 4 - Lagrangian Coherent Structures in the left ventricle of a healthy volunteer

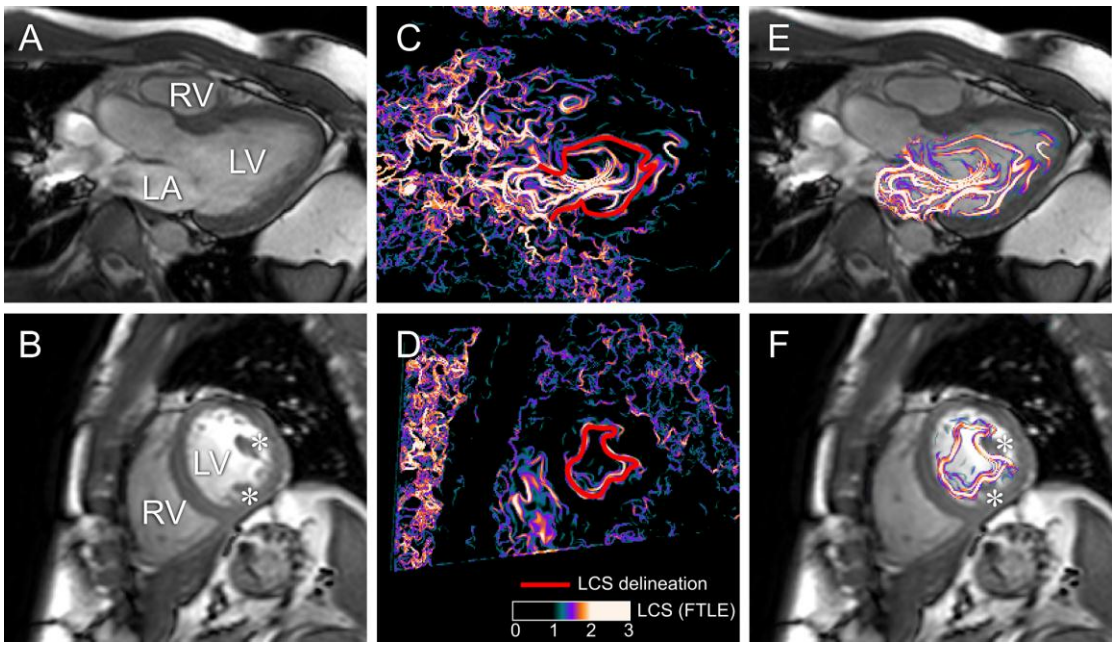

Lagrangian Coherent Structures (LCS) in the left ventricle of a healthy volunteer at the end of rapid filling (cf. Figure 3, Dt1). Panel A shows a three-chamber long-axis cine image. Panel B shows a mid-ventricular short-axis cine image. Note the papillary muscles (*). Panels C and D show cross-sections of the three-dimensional vortex ring LCS image in the three-chamber and short-axis views respectively. The red, solid line shows typical delineations of vortex ring LCS after rapid filling. Since the trailing edge of the vortex ring could not be identified, the leading edge was extrapolated to the atrioventricular plane along LCS originating from the mitral valve (Panel C). Panel E shows vortex ring LCS superimposed on the three-chamber cine image. Note how the vortex ring (shown as white/yellow lines) occupies a large part of the left ventricle. Panel F shows vortex ring LCS superimposed on the short-axis cine image. Note that the vortex ring LCS adapt to papillary muscles (*). Animated version of Panel E is available online in the supplemental files (volunteer 5).

LV = left ventricle, LA = left atrium, RV = right ventricle. Asterisks (*) = papillary muscles. Color scale: LCS. LCS are defined as lines of high Finite-Time Lyapunov Exponent (FTLE).

Figure 5 – Lagrangian Coherent Structures in a patient with dilated ischemic cardiomyopathy

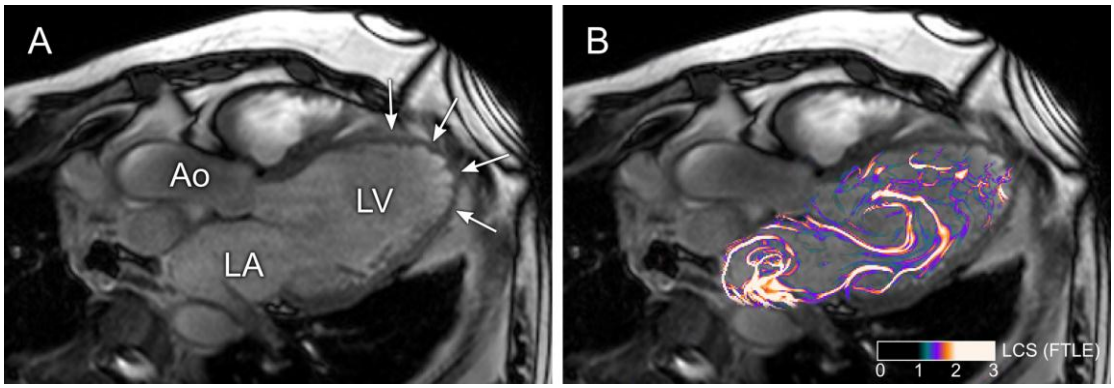

Lagrangian Coherent Structures (LCS) in the left ventricle of a patient with dilated ischemic cardiomyopathy at the end of rapid filling (cf. Figure 3, Dt1). Panel A shows a three-chamber view of the heart. Note the thin-walled apical aneurysm (white arrows). In panel B, a cross-section of LCS in the three-chamber view is shown. A vortex ring is clearly visible. It is qualitatively similar to the vortex rings found in healthy volunteers (Figures 4 and 6), but occupies a smaller part of the left ventricle. Animated version available online in the supplemental files (patient 2).

LV = left ventricle, LA = left atrium, Ao = aorta. Color scale: LCS. LCS are defined as lines of high Finite-Time Lyapunov Exponent (FTLE).

Figure 6 – Lagrangian Coherent Structures at different time phases during diastasis

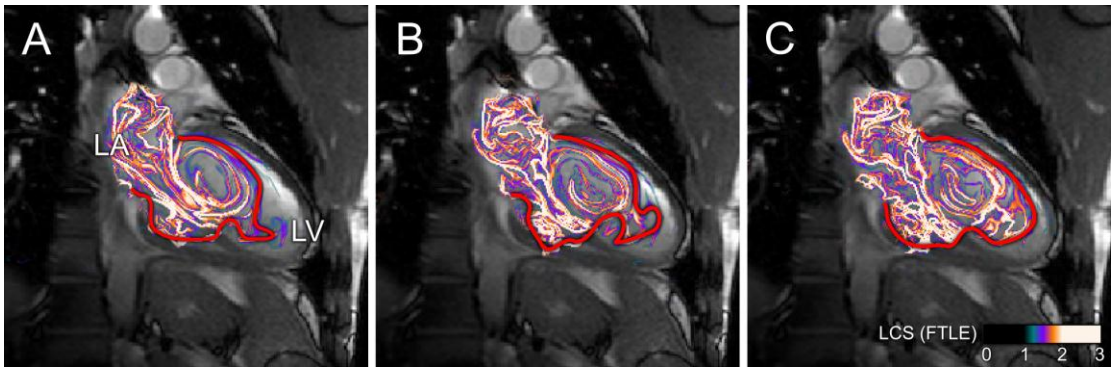

Lagrangian Coherent Structures (LCS) in the two-chamber view in one volunteer at three different time points during diastasis (cf. Figure 3). Red lines indicate the outer boundary of the vortex ring defined by LCS. Panel A shows LCS after rapid filling (Dt1). The LCS reveal a distinct asymmetric vortex ring, with a large vortex in the anterior part of the LV and a smaller vortex in the inferior part. Panel B shows LCS at mid-diastasis (Dt2), after organized transmitral flow has ended. The LCS continue to deform and while the vortex remains visible, it is less well defined. Panel C shows LCS before atrial contraction (Dt3). The LCS have deformed additionally and vortex structure is less well defined. Diastatic LV volume remains constant throughout. Note the proximity of the outer vortex boundary to the LV endocardium at all three time points. Animated version available online in the supplemental files (volunteer 2, 2-chamber view).

LA = left atrium, LV = left ventricle. Color scale: LCS. LCS are defined as lines of high FTLE (Finite-time Lyapunov Exponent).

Tables

Table 1. Subject characteristics

	Age (years)	Gender	Weight (kg)	Height (cm)	BSA (m^2)
Volunteers (n = 9) Mean ± SD	30 ± 9	6M, 3F	75 ± 13	180 ± 12	1.94 ± 0.23
Patients (n = 4) Mean ± SD	65 ± 11	3M, 1F	83 ± 9	177 ± 9	2.02 ± 0.15

Patients: Dilated ischemic cardiomyopathy. Body surface area (BSA) was computed with the Mosteller formula. SD = standard deviation. Individual data is available with the online version of this article as a supplemental file.

Table 2. Left ventricular volumes and parameters

	ESV (ml)	DV (Dt1) (ml)	EDV (ml)	EDV/BSA (ml m^{-2})	SV (ml)	EWV (ml)	EF	VFR
Volunteers (n = 9)	73 ± 17	164 ± 38	184 ± 40	94 ± 10	111 ± 26	91 ± 24	60 ± 4%	4.5±1.2
Patients (n = 4)	310±119	372±119	400±110	197±52	90±16	62±13	24±10%	3.3±1.0

ESV = End-systolic volume, DV = diastatic volume, measured at mid-diastasis (Dt1, cf. Figure 3), EDV = End-diastolic volume, EF = ejection fraction. SV = stroke volume, EWV= E-wave volume, defined as DV – ESV, BSA = Body surface area computed using the Mosteller formula. VFR = vortex formation ratio (vortex formation time, VFT, or stroke ratio L/D)[7]. Patients: Dilated ischemic cardiomyopathy. Individual data is available with the online version of this article. The was no statistically significant difference in VFR between volunteers and patients ($p = 0.11$). Results are presented as mean ± standard deviation. Individual data is available with the online version of this article as a supplemental file.

Table 3. Vortex volumes

	Dt1: After rapid filling	Dt2: Mid-diastasis	Dt3: Before atrial contraction
Volunteers, Groups 1&2 Mean ± SD	83 ± 20 ml 51 ± 6 %	-	-
Volunteers, Group 1 Mean ± SD	86 ± 22 ml 54 ± 5 %	91 ± 26 ml 57 ± 5 %	89 ± 21 ml 55 ± 4 %
Patients, Groups 1&2 Mean ± SD	74 ± 18 21 ± 5%	-	-
Patients, Group 1 Mean ± SD	80 ± 17 19 ± 4%	90 ± 15 22 ± 6%	93 ± 14 22 ± 6%

Volume of the vortex ring (VV), i.e. the volume inside the vortex ring LCS (observer 1). Percentages show vortex volumes relative to left ventricular volume at diastasis (DV). Subjects in Group 1 had a diastasis longer than 100 ms. Subjects in Group 2 had no diastasis or a diastasis shorter than 100 ms. SD = standard deviation. Patients: Dilated ischemic cardiomyopathy. Figure 3 shows the definition of the time phases Dt1, Dt2 and Dt3. Individual data is available with the online version of this article as Supplemental File 2.

Table 4. Interobserver and interstudy variability

	Bias (ml)	Bias (%)	p-value (Wilcoxon)
VV interobserver, volunteers (n = 9)			
Groups 1&2, Dt1	-1 ± 9	-1 ± 13%	1
Group 2, Dt1	3 ± 9	9 ± 11%	0.75
Group 1, Dt1	-2 ± 9	-4 ± 14%	0.84
Group 1, Dt2	-10 ± 7	-12 ± 9%	0.03
Group 1, Dt3	-6 ± 9	-9 ± 14%	0.22
VV interstudy 1.5T vs 3T, volunteers (n = 6)			
Observer 1, Dt1	-2 ± 11	-2 ± 12%	1
VV interobserver, patients (n = 4)			
Groups 1&2, Dt1	-7 ± 9	-7 ± 11%	0.25

Bias computed using Bland-Altman analysis. Group 1: Diastasis > 100 ms, (N = 6) Group 2: Diastasis < 100 ms (N = 3). VV = vortex volume. Dt1, Dt2 and Dt3 are defined in Figure 3. Note that the difference between observers was statistically significant only for Group 1, Dt2 in the volunteers.